Proceedings of SPIE, Volume 3964 Internet Imaging, Eds: G.B. Beretta & R Schettini, 26-28 January 2000, San Jose, CA, pp 196-206

Comparison of multispectral images across the Internet

Gerie W.A.M. van der Heijden[a], Gerrit Polder[ab], and Theo Gevers[c]

[a]CPRO, P.O.Box 16, 6700 AA Wageningen, the Netherlands
[b]Department of Pattern Recognition, Delft University of Technology, the Netherlands
[c]ISIS-group, Faculty of WINS, University of Amsterdam, the Netherlands

ABSTRACT

Comparison in the RGB domain is not suitable for precise color matching, due to the strong dependency of this domain on factors like spectral power distribution of the light source and object geometry. We have studied the use of multispectral or hyperspectral images for color matching, since it can be proven that hyperspectral images can be made independent of the light source (color constancy) and object geometry (normalized color constancy).
Hyperspectral images have the disadvantage that they are large compared to regular RGB-images, which makes it infeasible to use them for image matching across the Internet. For red roses, it is possible to reduce the large number of bands (>100) of the spectral images to only three bands, the same number as of an RGB-image, using Principal Component Analysis, while maintaining 99% of the original variation. The obtained PCA-images of the roses can be matched using for example histogram cross correlation. From the principal coordinates plot, obtained from the histogram similarity matrices of twenty images of red roses, the discriminating power seems to be better for normalized spectral images than for color constant spectral images and RGB-images, the latter being recorded under highly optimized standard conditions.

Keywords: PCA, flowers, roses, color matching, color invariance, spectroscopy, Flores, hyperspectral, multispectral, color constancy

1. INTRODUCTION

Several state-of-the-art image databases allow the comparison of a color image across the Internet with images in a database. Usually, color matching is computed in the RGB-domain. However, RGB-based comparison is not suitable for precise color matching due to the strong dependency of the RGB domain to recording conditions. Next to surface and reflection/absorption characteristics of the object, the light source (illumination intensity, direction and spectral power distribution), the sensitivity of the filters, the settings of the camera (like aperture), and the viewing position, all influence the final RGB-image. Color-(sub)domains exist which are more or less invariant to the various causes of color variation. Independence for the illumination intensity of the light source can be obtained by the use of color models with the intensity component eliminated, like normalized rgb or hue/saturation. Funt & Finlayson[1] describe a method to obtain color constancy independent of the color of the illumination. By taking ratios of colors of neighboring pixels, a color constant feature can be obtained, which is not only independent of the illumination color but also discounts shadows and shading cues[2]. Color invariance, however, comes at the price of reduced information, and in many cases, these color invariant systems do not offer enough discriminating power. It would be desirable to have a system which is invariant for variations due to light source and camera and has at least the discriminating power of RGB images taken under constant lighting conditions.

With multispectral or hyperspectral imaging[3], a large part of the electromagnetic spectrum e.g. between 380 and 700 nm, is recorded in more than hundred small bands (e.g. every 5 nm) for every pixel. Hyperspectral imaging offers the potential to combine color constancy with a high discriminating power. The disadvantage is that it increases the amount of data enormously and hyperspectral images of tens of megabytes are simply too large to be sent over the Internet for image matching. Computational methods are required to reduce the data before sending.

The application in this paper for which the possibilities of hyperspectral imaging are investigated is the granting of Plant Breeders' Rights (PBR) for ornamental (flowering) rose-varieties. Before a new candidate variety can be granted PBR (kind of patent), it has to be declared distinct from all other existing varieties worldwide. Therefore, in every country which examines a new variety application, the candidate variety has to be compared with existing varieties, not only in the same country but also in all other countries. For roses, international guidelines exists which makes it possible to describe a variety

in a standardized way using a large number of well-agreed features[4]. These descriptions are used for the comparison, but are often not sufficient: the differences in color and color patterns can be small and are difficult to describe. Therefore real flowers or high quality color images are also required for comparison. There is a considerable need for a system which allows image comparison of new variety applications with an up to date digital reference collection.
Therefore a distributed image database system, FLORES™, has been developed in the Netherlands[5]. It runs from the web-browser and uses Java applets to allow RGB-color image matching across the Internet. Hence the user can compare his own images with a central database. In the applet, tools are available for semi-interactive segmentation (like thresholding and region-growing) of an image in an object (flower) and background. When the user is satisfied with the segmentation, the image and segmentation mask are sent to a central database, where feature extraction and matching takes place. The central database returns a list of thumbnail pictures of the most resembling images in decreasing order of similarity. The thumbnails contain links to larger-size images and other variety information.
Color differences between varieties can be rather subtle ($\Delta E \approx 1$ can be sufficient for variety distinction) and variation caused by recording conditions (camera, light source) can seriously disturb the comparison. Therefore we are studying the use of hyperspectral images for plant variety testing with respect to the following four criteria:

1. color independent of the spectral power distribution (SPD) of the light source
2. color independent of the object geometry
3. compact set of features for transmission over the Internet
4. high discriminating power for the color matching

The paper is outlined as follows. In section 2, the material and recording conditions are discussed. Section 3 describes the theory to obtain spectral images independent of the SPD of the light source and object geometry. In section 4, a compact and discriminative set of features are presented for reducing the transmission load over the Internet. In section 5, a measure of similarity is presented to compare the images. Results of the roses experiment will be presented in section 6 and finally the discussion will be given in section 7.

2. MATERIALS AND METHODS

Twenty images of flowers of close resembling varieties of dark red roses are used for this experiment. The roses were grown in a greenhouse under standard Dutch conditions and flowers were picked in August 1999. It should be stressed that color differences between the flowers are very small. If the method is capable of correctly distinguishing the varieties under these very demanding conditions, it has a large potential.
The flowers were recorded in two ways:

- with an RGB-color camera (Sony DX-950P 3-CCD). The light source consists of high frequency fluorescent daylight tubes (6500 K). The framegrabber used is a Matrox Meteor.
- with a hyperspectral recording system which consists of an ImSpector V9 spectrograph (Specim, Finland), connected to a B/W CCD-camera (Hitachi, KP-M1, IR-cutoff filter removed) and equipped with a NIKON 55mm-lens. The light source is Tungsten halogen. The framegrabber is a Matrox Meteor II.

The ImSpector is a straight axis imaging spectrograph using a prism-grating-prism (PGP) dispersive element and transmissive optics[6,7]. Most other imaging spectrographs have a folded optical path, which makes coupling to a camera system more complicated than it would be with a straight axis component, like a lens. Off axis configuration also causes astigmatism and other aberations. With the PGP dispersive element, these problems are largely overcome, due to the axial transmissive spectrograph optics, made possible by a holographically recorded transmission grating. The ImSpector V9 has a spectral range of 430-900 nm. The slit size is 50 □m.
The ImSpector uses one axis of the CCD-chip as the spatial axis and the other as the spectral axis. To record a spatial two-dimensional image, the object has to be moved with respect to the camera. Therefore we have built a system consisting of a linear translation table (Lineartechniek), driven by a programmable microstepping step motor driver (Ever Elettronica, Italy).
The hyperspectral images are binned to reduce the size of image. The binning in the spatial axis is a factor 2. The step size of the stepper table was chosen to match the spatial resolution. The resulting images have a spatial dimension of 256x256 square pixels (resolution 0.5mm/pixel). In the spectral axis a binning factor is chosen, such that a spectral resolution of 170 bands (from 430-900 nm) remains.
The software to control the stepper table and framegrabber, to construct the hyperspectral images and to save and display them has all been locally developed in the Java-language. Further image processing is done in Scil-Image (TNO-TPD, Delft, NL) and data analysis in Genstat (IACR, Rothamsted, UK).

3. COLOR INVARIANCE

The spectra obtained by the spectrograph depend on the light source and object characteristics. Therefore, these spectra may vary with a change in the intensity and energy distribution of the light source, material characteristics and viewing mode. The aim of this section is to propose spectra which are invariant to illumination (color constancy) and the object geometry and shadows (normalization). We will follow the method proposed by Stokman & Gevers[8].
The section is outlined as follows. In section 3.1, the reflection is given modeling interaction between light and matter. Color constant spectra are presented in Section 3.2. Then, the color constant spectra are made independent of object geometry and shading (normalization) in Section 3.3.

3.1 The Reflection Model

Let $E(\vec{x},\lambda)$ be the spectral power distribution of the incident (ambient) light at the object surface at $\vec{x}$ and let $L(\vec{x},\lambda)$ be the spectral reflectance function of the object at $\vec{x}$. The spectral sensitivity of the *k*th sensor is given by $F_k(\lambda)$. Then ρ_k, the sensor response of the *k*th channel, is given by:

$$\rho_k(\vec{x}) = \int_\lambda E(\vec{x},\lambda)L(\vec{x},\lambda)F_k(\lambda)d\lambda \tag{1}$$

where λ denotes the wavelength, and $L(\vec{x},\lambda)$ is a complex function based on the geometric and spectral properties of the object surface. The integral is taken from the visible spectrum (e.g. 380-700 nm).
Further, consider an opaque inhomogeneous dielectric object, then the geometric and surface reflection component of function $L(\vec{x},\lambda)$ can be decomposed in a body and surface reflection component as described by Shafer[9]:

$$\phi_k(\vec{x}) = G_B(\vec{x},\vec{n},\vec{s})\int_\lambda E(\vec{x},\lambda)B(\vec{x},\lambda)F_k(\lambda)d\lambda + G_S(\vec{x},\vec{n},\vec{s},\vec{v})\int_\lambda E(\vec{x},\lambda)S(\vec{x},\lambda)F_k(\lambda)d\lambda \tag{2}$$

giving the *k*th sensor response. Further, $B(\vec{x},\lambda)$ and $S(\vec{x},\lambda)$ are the surface albedo and Fresnel reflectance at $\vec{x}$ respectively. $\vec{n}$ is the surface patch normal, $\vec{s}$ is the direction of the illumination source, and $\vec{v}$ is the direction of the viewer. Geometric terms G_B and G_S denote the geometric dependencies on the body and surface reflection component respectively.

3.2 Color Constancy

Consider the reflectance of a perfect reflecting white diffuser. A sample is called a perfect white when the sample diffusely reflects all wavelengths of the light source and does not absorb any of them. Diffuse reflectance implies that the reflected light is symmetrical in all directions. The white diffuser used in this paper is a white tile of PTFE-plastic with a spectral reflectance of over 0.98 from 400 till 1500 nm. Hence, we may assume that the white diffuser has constant spectral albedo reflectance $B(\vec{x},\lambda) = 1$. Further, having diffuse reflectance and assuming that the surface normal $\vec{n}$ is equal to the viewing direction $\vec{s}$, then $G_B(\vec{x},\vec{n},\vec{s}) = 1$. Then the sensor response of the *k*th channel of the white reference sample (without specularities) is given by:

$$\phi_k(\vec{x}) = \int_\lambda E(\vec{x},\lambda)F_k(\lambda)d\lambda \tag{3}$$

In this way, the relative spectral power distribution of the white reference is measured.
Further, an image is captured of an arbitrary sample under the same illumination conditions, and is divided by the previously obtained recording of the illuminant. We thus have:

$$\phi_k(\vec{x}) = \frac{G_B(\vec{x},\vec{n},\vec{s})\int_\lambda E(\vec{x},\lambda)B(\vec{x},\lambda)F_k(\lambda)d\lambda}{\int_\lambda E(\vec{x},\lambda)F_k(\lambda)d\lambda} + \frac{G_S(\vec{x},\vec{n},\vec{s},\vec{v})\int_\lambda E(\vec{x},\lambda)S(\vec{x},\lambda)F_k(\lambda)d\lambda}{\int_\lambda E(\vec{x},\lambda)F_k(\lambda)d\lambda} \tag{4}$$

giving the *k*th sensor response of a sample with respect to a white reference. As mentioned before, the filters $F_k(\lambda)$ are narrow-band filters, through the use of the spectrograph. In fact, filter $F_k(\lambda)$ can be modeled as a unit impulse that is shifted over *N* wavelengths: the transmission at λ_k=λ and zero elsewhere. This allows us to rewrite equation (4) as:

$$\phi_k(\vec{x}) = \frac{G_B(\vec{x},\vec{n},\vec{s})E(\vec{x},\lambda_k)B(\vec{x},\lambda_k)}{E(\vec{x},\lambda_k)} + \frac{G_S(\vec{x},\vec{n},\vec{s},\vec{v})E(\vec{x},\lambda_k)S(\vec{x},\lambda_k)}{E(\vec{x},\lambda_k)} \tag{5}$$

obtaining:

$$\phi_k(\vec{x}) = G_B(\vec{x},\vec{n},\vec{s})B(\vec{x},\lambda_k) + G_S(\vec{x},\vec{n},\vec{s},\vec{v})S(\vec{x},\lambda_k) \quad (6)$$

Equation (6) implies that, under the assumption of a unit impulse band filter, the spectral images obtained by the spectrograph can be made independent of the illuminant by dividing the original spectral image by the spectral transmittance of the illuminant. Note that the spectral power distribution of the light source is unimportant as long as it contains all wavelengths of the visible light in a sufficient amount.
However, in practice, the color filters are never unit impulse band filters. Further, the perfect white diffuser can only be approximated by a real material. Under the assumption that natural objects and light sources, due to physics restrictions, have relatively smooth spectral power distributions, we might still be able to approximate equation (6).

As said before, the white reference image used in this paper has been taken from a white tile of PTFE-plastic with a spectral reflectance of over 0.98 from 400 till 1500 nm. Before dividing the spectra by the white reference the dark current has been subtracted. The dark current was obtained by taking an image with a closed lens cap and lights turned off.

3.3 Normalization

In this section, the color constant spectra are normalized yielding spectra which are independent of the object geometry.
Consider the body reflection term of equation (6) :

$$D_k(\vec{x}) = G_B(\vec{x},\vec{n},\vec{s})B(\vec{x},\lambda_k) \quad (7)$$

giving the *k*th sensor response of the spectral reflectance curve of a matte surface.
According to equation (7), the color depends only on surface albedo and the brightness on factor $G_B(\vec{x},\vec{n},\vec{s})$. As a consequence, a uniformly painted surface may give rise to a broad variance of sensor values due to the varying circumstances induced by the image-forming process such as a change in object geometry.
In contrast, normalized sensor space is insensitive to surface orientation, illumination direction and intensity by dividing each channel by the sum of channels as follows from:

$$C_k(\vec{x}) = \frac{D_k(\vec{x})}{D_1(\vec{x}) + D_2(\vec{x}) + ... + D_N(\vec{x})} =$$

$$\frac{G_B(\vec{x},\vec{n},\vec{s})B(\vec{x},\lambda_k)}{G_B(\vec{x},\vec{n},\vec{s})\big(B(\vec{x},\lambda_1) + B(\vec{x},\lambda_2) + ... + B(\vec{x},\lambda_N)\big)} = \quad (8)$$

$$\frac{B(\vec{x},\lambda_k)}{B(\vec{x},\lambda_1) + B(\vec{x},\lambda_2) + ... + B(\vec{x},\lambda_N)}$$

taken over *N* wavelengths and only dependent on the surface albedo and independent of the illumination spectral power distribution, illumination direction $\vec{s}$, and object geometry $\vec{n}$.

4. CONSTRUCTION OF PCA-IMAGE

To satisfy criterion 3, we try to reduce the number of bands to an acceptable number. For this, we use principal component analysis (PCA). PCA finds orthogonal linear combinations of a set of features (spectral bands) that maximize the variation contained within them, thereby displaying most of the original variability in a smaller number of dimensions. It operates on the sums of squares and products matrix, formed from the original features.
In order not to include the variation due to differences between flower and background, only the pixels of the flowers were considered. The object (flower) in each of the spectral images was located by applying a threshold on a spectral band in the red region. Since there was hardly any variation in the background, fixed thresholding worked fine for all images recorded, but in principle any segmentation method can be applied, including interactive methods. The hence obtained binary mask was used for selecting only the pixels belonging to the flower.
A sum of squares and products matrix ($\sum(x_{ip}$-mean(x_i)$)(x_{jp}$-mean(x_j)$)$) is formed by combining all pixels *p* belonging to a flower over all images considered, treating each spectral band *i* as a separate feature x_i. This results in a 170x170 symmetric matrix, with the sum of squares of the features on the main diagonal and the cross products on the off-diagonals.

After construction of the matrix, the eigenvalues and eigenroots of this sum of squares and product matrix were extracted.

The feature vector x=(x_1, x_2, …, x_{170}) at every pixel can now be replaced by a reduced feature vector y=(y_1, y_2, …y_N) with N<<170, where y_i can be calculated as the product of the original feature set x with eigenvector j.
This can be done for each every pixel in each image, resulting in a 256x256xN image.

5. IMAGE MATCHING

To calculate a measure of color similarity between flowers, an N-dimensional histogram H was constructed for each flower. The number of bins and bin size in each dimension depends on the observed range of values in each principal component, over all images. Therefore the maximum and minimum value were calculated over all images for each of the three components. The bin size of the histogram in each dimension was taken as the ratio of the observed range over all flowers divided by the number of bins per component.
We have used a similarity measure S between histograms H_A and H_B as defined on the basis of symmetric cross correlation:

$$S(H_A, H_B) = \sum_{i=1}^{N} \sum_{j=1}^{nrbin_i} H_A(i,j) H_B(i,j) / \tfrac{1}{2}\{(H_A(i,j))^2 + (H_B(i,j))^2\} \quad (9)$$

where $H(i,j)$ is the number of pixels in bin j in dimension i, divided by the total number of pixels summed over all bins and dimensions, i.e. the relative frequency of bin(i, j).
For the RGB images, the same histogram binning (64x64x64 bins) and similarity measures were applied.

To obtain insight in the structure and relationship in the similarity matrix, a Principal Coordinates Analysis (PCO) is performed. The Principal Coordinates of a symmetric distance or similarity matrix are orthogonal features, which try to capture the original distances in the matrix in as few features as possible. In a PCO-plot of the first and second Principal Coordinate, the multi-dimensional distances (or similarities) between the objects are optimally represented in a two-dimensional plane.

6. RESULTS

The spectral images are analyzed in two ways. One is based on color constant spectral images as described in section 3.2, the other on normalized color constant spectral images as described in section 3.3
For the color constant spectra, the first three eigenvectors of the sum and squares and cross products matrix contained more than 99% of the total variation as can be seen by the cumulative contribution of the eigenvalues (Table 1). Therefore the 170 bands of every pixel can be reduced to 3 bands (principal components), while maintaining over 99% of the original variation. This means a size reduction of 167/170 = 98.2% compared to the original image size.
For the normalized spectral images, the first three components maintained over 98.5% of the total variation.

Table 1. The value of the first five eigenvalues, their relative contribution and their cumulative contribution to the total variation (sum of all eigenvalues) of the color constant spectra and of normalized color constant spectra.

eigenvector	color constant spectra			normalized spectra		
	eigenvalue $*10^6$	% variation	cum. %	eigenvalue $*10^6$	% variation	cum. %
1	123467	95.14	95.14	664982	87.94	87.94
2	4564	3.52	98.66	48492	6.41	94.35
3	965	0.74	99.40	31997	4.23	98.58
4	206	0.16	99.56	2623	0.35	98.93
5	85	0.07	99.63	1226	0.16	99.09

Images of the first, second and third principal component are shown in Figure 1 and 2. In Figure 1, the principal components are based on color constant spectra. The images were scaled between 0 and 255 for each component, using the same scaling per component over all the images. All the flowers exhibited almost the full range for the first component, being bright at the border and dark in the middle. This indicates that this component is more suitable of capturing differences within a flower than between flowers. These differences are probably due to object geometry. For the second component more differences between flowers can be observed.

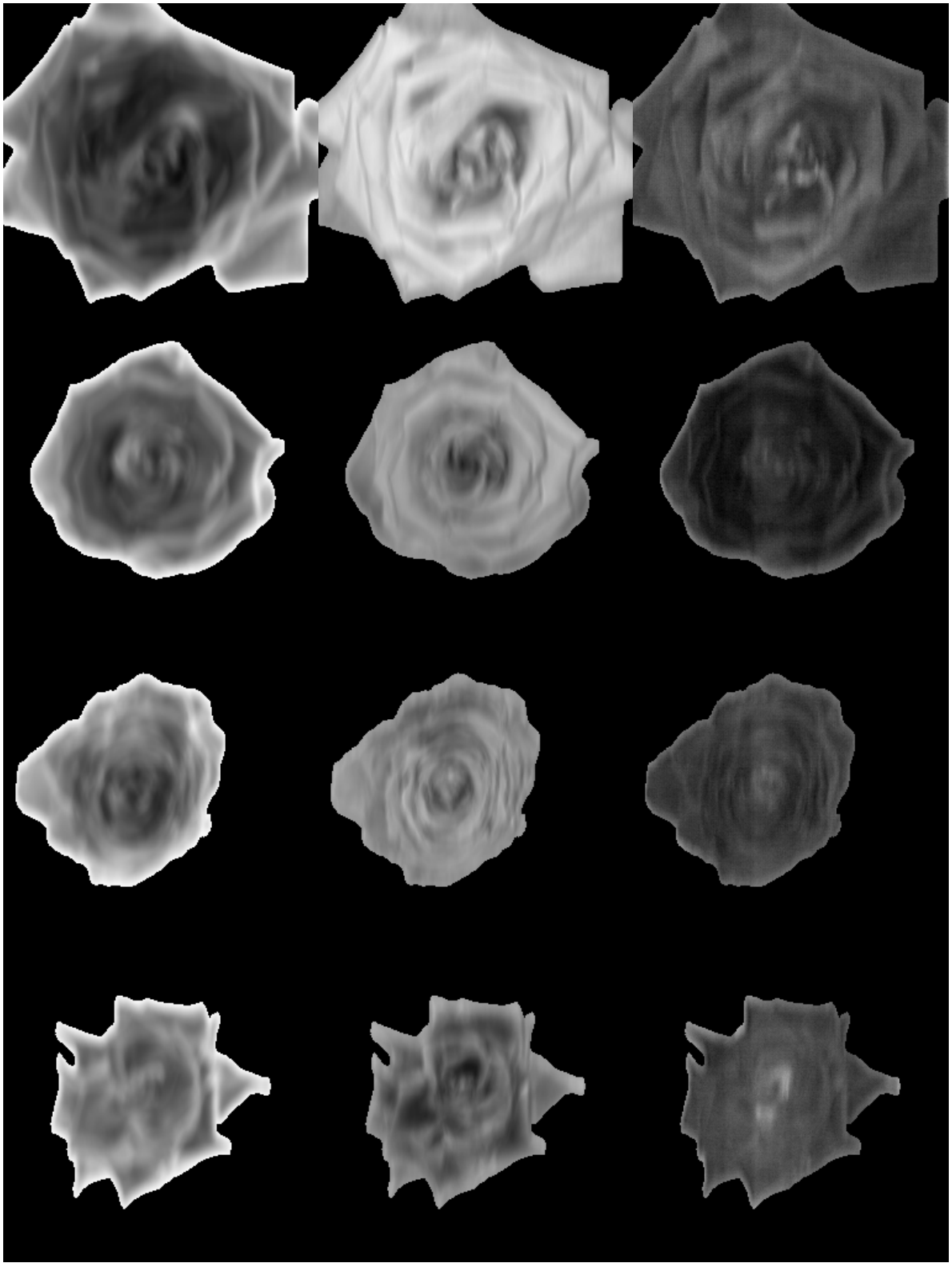

Figure 1. The first three principal components (columns) of four different rose-flowers (rows) using color constant spectra. The left column represents the first principal component, the middle column the second, and the right column the third component. For comparison with Figure 3-5: the labels of the images from top to bottom are 657_1, 564_1, 549_1, 258_1.

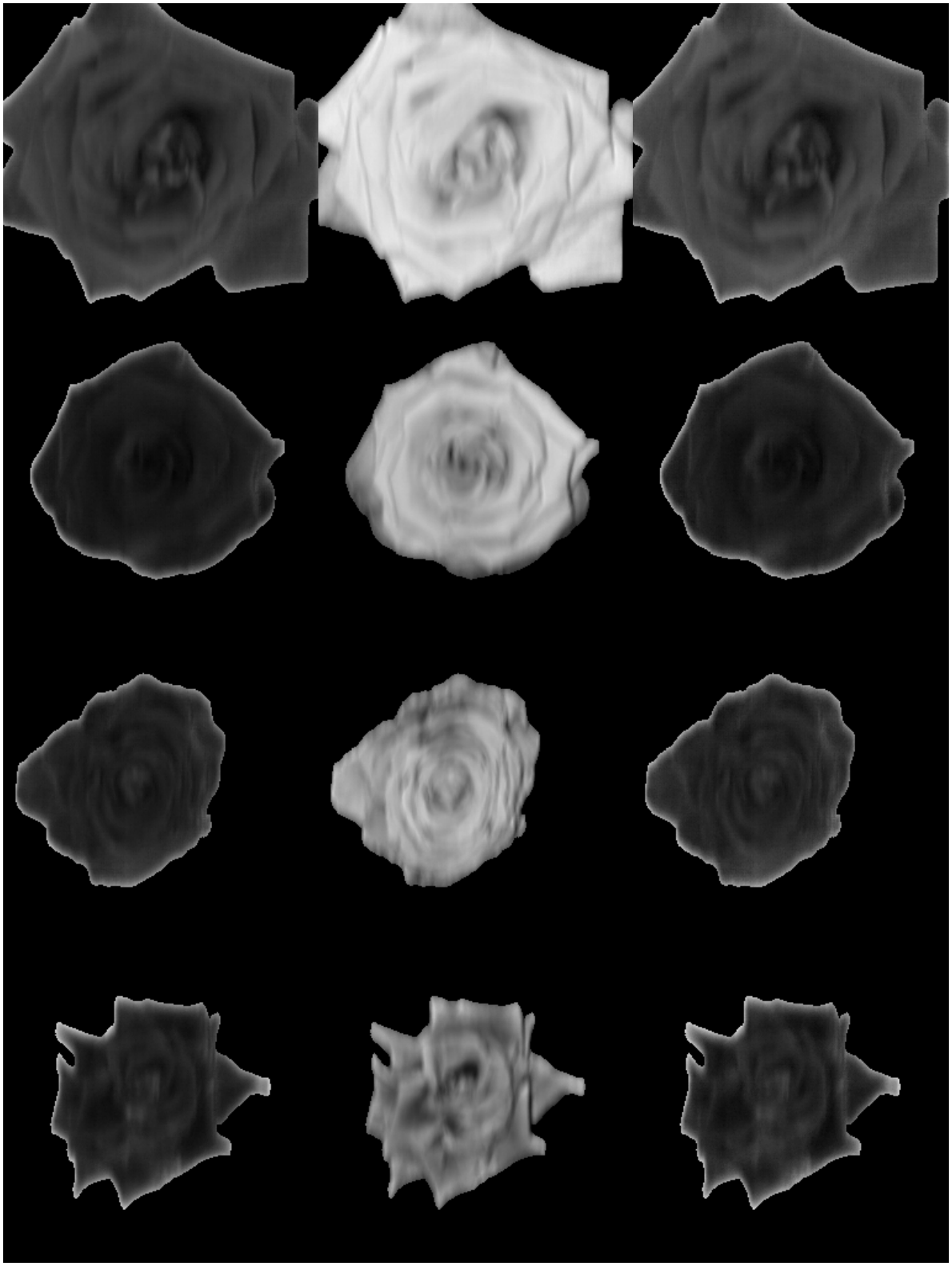

Figure 2. The first three principal components (columns) of four different rose-flowers (rows), using normalized spectra. The left column represents the first principal component, the middle column the second, and the right column the third component. For comparison with Fig 3-5: the labels of the images from top to bottom are 657_1, 564_1, 549_1, 258_1.

For the normalized spectra (Figure 2), the first component is clearly less influenced of the object's geometry.

From the PCA-images of both color constant spectra and normalized color constant spectra, 3-D histograms were formed, using the same binary mask for the flower as was used for the construction of the sum of squares and cross products matrix. The number of bins for all three components was set at 64, yielding a histogram of size 64x64x64. This same histogram was used for the RGB-images.

In Figures 3-5, PCO-plots are shown for the histograms calculated from the PCA-images and the RGB-images. The Minimum Spanning Tree is overlaid on the plot. The Minimum Spanning Tree connects the nearest neighbors in the multi-dimensional space. It serves as an indicator of the goodness of fit of the two-dimensional representation of the multi-dimensional space. If many lines are crossing the 2D-representation is not good. The Minimum Spanning Tree has the same structure as the hierarchical nearest neighbor tree.
The percentage of variance contained within the similarity matrix formed from the histograms of the PCA-images from color constant spectra was explained for 22% by the first coordinate and for 15% by the second coordinate, giving a combined explanation of 37% of the total variation in the matrix.

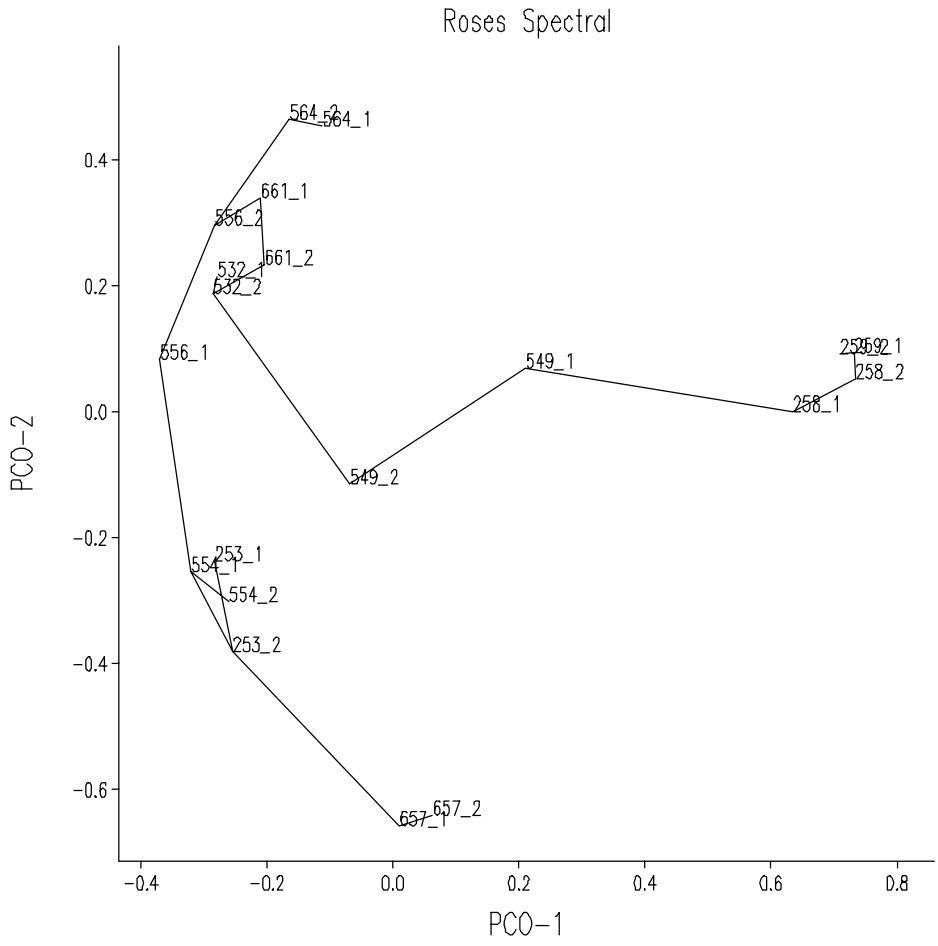

Figure 3. The Minimum Spanning Tree (the straight lines) is overlaid on first two principal scores of twenty rose flowers, extracted from the matrix formed from the histograms of the PCA-images of color constant spectra. The flowers are labeled by their plant number, followed by an underscore and a flower number.

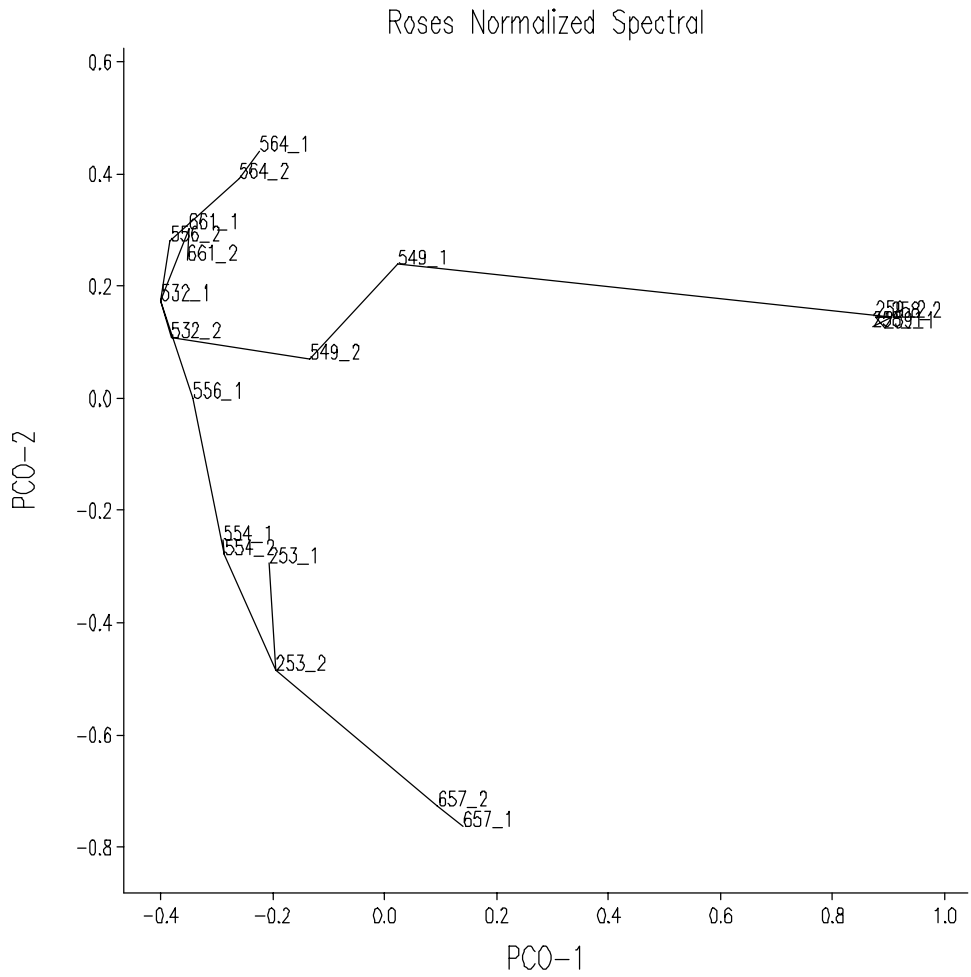

Figure 4. The Minimum Spanning Tree (the straight lines) is overlaid on first two principal scores of twenty rose flowers, extracted from the matrix formed from the histograms of the PCA-images of normalized spectra. The flowers are labeled by their plant number, followed by an underscore and a flower number.

For the PCA-images of the normalized color constant spectra, the first coordinate explained 36% and the second 19% of all variation in the similarity matrix (55% combined).
For the RGB-images, these numbers were 49% and 24% respectively (73% combined).

From these figures, it can be seen that the two flowers of the same plant all lie close together, illustrating that the same plant gives the same color. Plant 258 and 259 belong to the same variety and the four points of this variety all lie together at the utmost right side in the plot for all three methods. It can be concluded that differences between plant of the same variety are similar to differences between flowers of the same plant. This is to be expected, since the growing conditions are highly controlled and uniform and all plants of the same variety are genetically identical. Therefore it is possible to use small color differences for discriminating varieties.
Furthermore all three figures clearly show several distinct groups of flowers. These groups are however not identical for the three methods. With color constant spectra (Figure 3), flowers of plant 253 were not distinguishable from plant 554. With RGB images (Figure 5) they could easily be distinguished. With normalized spectra (Figure 4), plant 253 is close to 554, but flowers of the same plant are still nearest neighbors and there is some distinction.
With RGB images, plant 554 could not be distinguished from plants 556 and 564, but for both spectral method this was not a problem.
Therefore RGB and PCA images do not contain the same information. Some information in the RGB images is not present in the PCA-images, and vice versa.

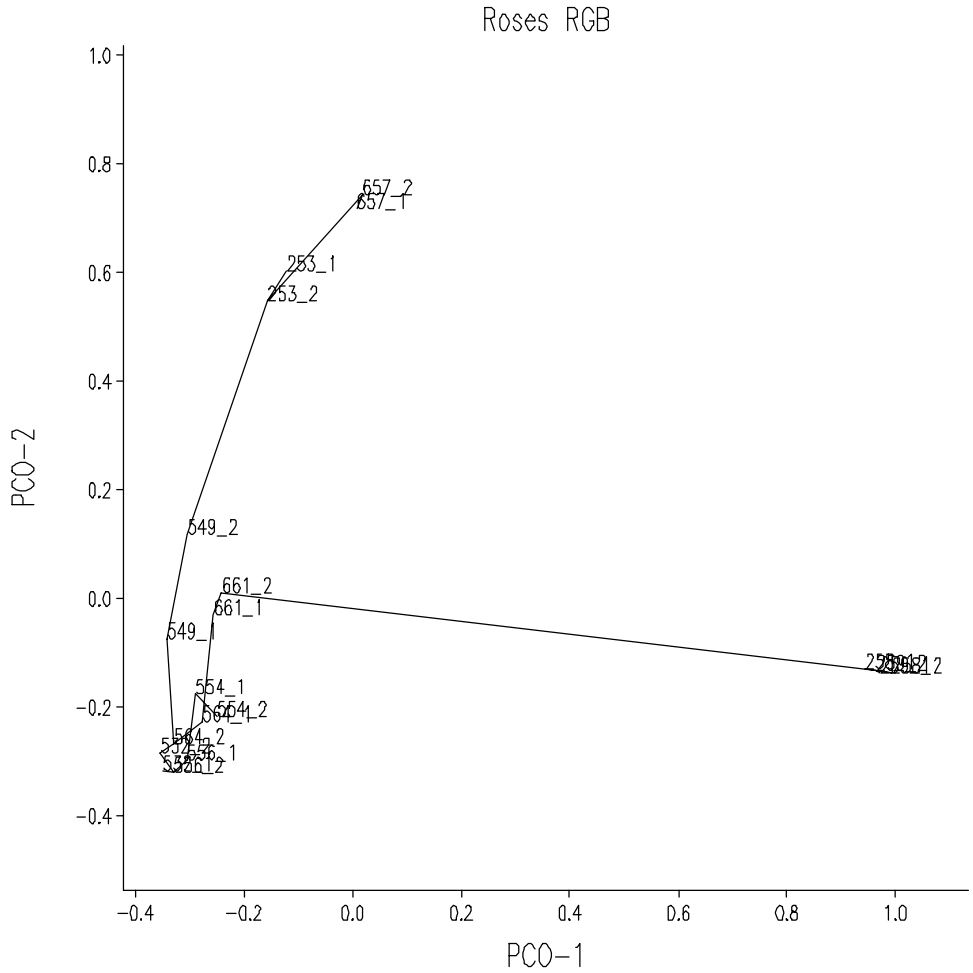

Figure 5. The Minimum Spanning Tree (the straight lines) is overlaid on first two principal scores of twenty rose flowers, extracted from the matrix formed from the histograms of the RGB-images. The flowers are labeled by their plant number, followed by an underscore and a flower number.

7. DISCUSSION

The goal of this research was to develop a method to compare color images, where (1) the color of the flower was independent of the light source, (2) the color was preferably independent of object geometry, (3) the image was compact enough for comparison across the internet and (4) the discriminating power was at least similar to that of RGB-images recorded under highly optimized standard conditions.

The use of hyperspectral images allowed us to obtain color independence with respect to the light source and, after normalization, also to object geometry. Therefore we could fulfill the first tow criteria.

The PCA method allowed a 98% size-reduction of the hyperspectral image from 170 bands to only three bands, no more than an RGB-image. Hence it also fulfilled the third criterion.

Furthermore, the PCA method can simply be incorporated in a Java applet and current Java Just In Time compilers opposes no problem with regard to speed of calculation. The remaining obstacle for the use of hyperspectral images is the required scanning of the flower.

We have only studied Principal Component Analysis as a way to reduce the number of bands. This approach tries to preserve the overall variation, but makes no attempt to optimize the variation between different rose varieties. It might be that the use of other computational method like canonical variate analysis or partial least squares may give better results.

We did not compare white or pink roses with the red roses in this experiment, as this comparison will cause no problems. Matching problems will only occur in the same color groups. Nevertheless, the method should also work for other colors. The eigenvectors extracted from the set of dark red roses, will not be optimal for other colors. We can solve this by trying to calculate the PCA over the whole color set of roses and take more bands, or alternatively calculate an optimal PCA-set for every color group and do a preliminary calculation of the color of the flower. Based on this first rough grouping, the applet can ask the server for the optimal set of eigenvectors for this color group. If the main color of the rose is not clear-cut, e.g. containing red and pink spots, several sets of eigenvectors may need to be sent across the network to allow matching with different color groups.

We have used the spectral imaging for a very demanding problem, comparing dark red rose varieties with very limited color differences. Nevertheless, the spectral images seem to have at least the same discriminating power as optimally recorded RGB images. Since the hyperspectral images are independent of the illumination source, hyperspectral images are to be preferred. In the normalized spectral image, the color difference due to object geometry has also been eliminated. The results indicate that the normalized spectral images give at least the same, if not better, results than the color constant spectral images and RGB-images. The test set is too small to draw firm conclusions, but it seems that normalized spectral images are to be preferred above other images. A more extensive experiment including other color groups and more flowers would be necessary to confirm these preliminary promising results.

REFERENCES

1. B.V. Funt, and G.D. Finlayson. “Color constant color indexing” *IEEE PAMI* **17**(5), pp 522-.529. 1995.
2. T. Gevers, and A.W.M. Smeulders, “Color based object recognition” *Pattern Recognition* **32**, pp. 453-464. 1999.
3. D.A. Landgrebe, “Information Extraction Principles and Methods for Multispectral and Hyperspectral Image Data”, In *Information Processing for Remote Sensing*, C. H. Chen ed., Chapter 1. World Scientific, River Edge NJ 07661, 2000.
4. Anonymous. “Guidelines for the conduct of tests for distinctness, homogeneity and stability. Rose (Rosa L.)”, *UPOV document TG/11/7*, UPOV, Geneva, 1990.
5. G.W.A.M. van der Heijden, G. Polder, and J.W. van Eck. “Flores: a image matching database for ornamentals” In *Visual Information and Information Systems (Lecture Notes in Computer Science 1614).* P. Huijsmans & A. Smeulders, eds., pp 641-648, Springer, Berlin, 1999.
6. E. Herrala, and J. Okkonen, “Imaging spectrograph and camera solutions for industrial applications”, *International Journal of Pattern Recognition and Artificial Intelligence* **10** (1) pp 43-54, 1996.
7. H. Timo, E. Herrala, and A. Dall'Ava, “Direct sight imaging spectrograph: a unique add-on component brings spectral imaging to industrial applications”, *SPIE symposium on Electronic Imaging*, Vol. 3302, 1998.
8. H. Stokman, and T. Gevers. “Hyperspectral edge detection and classification”. *The Tenth British Machine Vision Conference*, Nottingham, September, 1999.
9. S.A. Shafer. “Using color to separate reflection components”, *COLOR Res. Appl.* **10**(4). pp 210-218, 1985.